AD-A070 598 MARYLAND UNIV COLLEGE PARK DEPT OF PHYSICS AND ASTRONOMY F/G 20/9
LINE STRENGTHS, COLLISON STRENGTHS AND EXCITATION RATES FOR MUL--ETC(U)
MAR 77 J DAVIS, P C KEPPLE, M BLAHA N00014-75-C-0309

UNCLASSIFIED NL

1 OF 1
AD
A070598

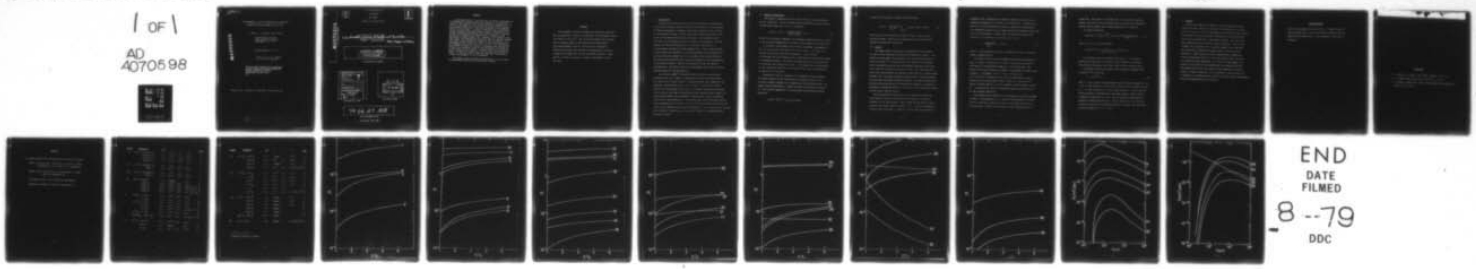

END
DATE FILMED
8 -79
DDC

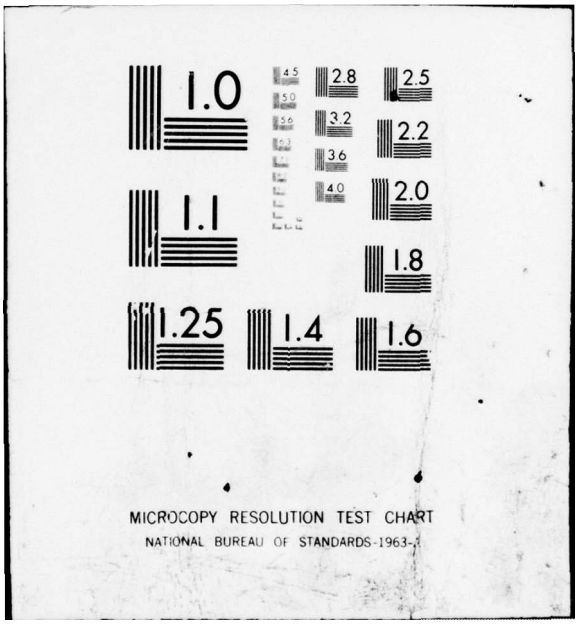
1.0
1.1
1.25
1.4
1.6
1.8
2.0
2.2
2.5
2.8
3.2
3.6
4.0
4.5
5.0
5.6
MICROCOPY RESOLUTION TEST CHART
NATIONAL BUREAU OF STANDARDS-1963-A

Code 6702

LINE STRENGTHS, COLLISION STRENGTHS AND EXCITATION RATES FOR MULTIPLY-CHARGED SILICON IONS

J. Davis, P. C. Kepple, and M. Blaha*

Plasma Physics Division
Naval Research Laboratory
Washington, D.C. 20375

(Received March 11, 1977)

APPROVED FOR PUBLIC RELEASE
DISTRIBUTION UNLIMITED

AD A070598

Work on this report was supported by ONR Contract N00014-75-C-0309 and/or N00014-67-A-0239 monitored by NRL 6702.02.

*Physics Dept., University of Maryland, College Park, Md.

79 06 27 008

DDC PROCESSING DATA

PHOTOGRAPH

THIS SHEET

RETURN TO DDA-2 FOR FILE

II

LEVEL

1

INVENTORY

AD A070598

DDC ACCESSION NUMBER

Line Strengths, Collision Strengths and Excitation - - - -

DOCUMENT IDENTIFICATION

Davis, Kepple, and Blaha

DISTRIBUTION STATEMENT A

Approved for public release;
Distribution Unlimited

DISTRIBUTION STATEMENT

Accession For

NTIS GRA&I [X]

DDC TAB [ ]

Unannounced [ ]

Justification

By

Distribution/

Availability Codes

Dist.	Avail and/or special
A	

DISTRIBUTION STAMP

DDC
RECEIVED
JUN 29 1979
D

DATE ACCESSIONED

79 06 27 308

DATE RECEIVED IN DDC

PHOTOGRAPH THIS SHEET

RETURN TO DDA-2

Synopsis

An important method of investigating the physical properties of high-temperature laboratory and solar plasmas is the analysis of optically thin spectral lines emitted by multiply-charged ions. In addition, the energy loss due to the emitted far ultraviolet and x-ray radiation may have a significant influence on the dynamical behavior of the plasma. In order to understand and interpret the optical emissions from these plasmas requires a knowledge of the various processes contributing to the observed spectra. One such process, and oftentimes the dominant one, is electron impact excitation of highly-charged ions. Because of the paucity of both experimental and theoretical cross section data for multiply-charged ions, there is an overwhelming demand for this information. In this paper we have calculated a number of selected transitions in multicharged silicon ions from Si VI to Si XIV. The calculations were carried out using the method of distorted waves ignoring the effects due to exchange except for the excitations in heliumlike Si XIII, where it was included. Included in the calculations are values for the line strength, collision strength and excitation rates. In addition, some of these rate have been represented by a simple two parameter fit for convenience.

This paper is being submitted for publication to the Journal of Quantitative Spectroscopy and Radiative transfer.

79 06 25 303

Abstract

Line strengths, collision strengths and excitation rates have been calculated for a variety of transitions in multicharged silicon ions from Si VI to Si XIV. The collision strengths were evaluated in an LS coupling scheme in the distorted wave approximation neglecting exchange except for the helium-like transitions. Excitation rates were then obtained by integrating the collision strength over a Maxwellian velocity distribution function. These results are then described by a simple two-parameter fit for the rates.

I. Introduction

The radiative emissions produced from high temperature laboratory and solar plasmas contains a potential wealth of information on such parameters as chemical composition, temperature and density structure, and a measure of the radiative cooling. However, before any reliable quantitative information can be deduced from the observed spectra, some knowledge must be available on the fundamental processes leading to its formation. One such process, and often the dominant one in an optically thin plasma, is electron-impact excitation of highly charged ions. Since a large fraction of the emitted line radiation is a direct consequence of the interaction of electrons and multi-charged ions, it is essential that accurate values of the cross sections and excitation rates be available for the interpretation of the observed spectra. Because of the paucity of both experimental and theoretical cross-section data for multi-charged ions, there is an overwhelming demand for this information.

In an earlier paper,[1] we provided values of the cross sections and excitation rates for a number of transitions in various ionization stages for several ions of solar interest: in particular, iron, neon, magnesium, and aluminum. Maintaining the spirit of this paper, we will present similar results for multi-charged silicon ions. In an ideal situation, it would make sense to obtain these data by employing the best available method, namely, the close-coupling method with correlation. However, this would be impractical in the case of many transitions. On the other hand, the distorted-wave method (DW) is appropriate for ionized systems and has an anticipated accuracy that increases as the charge on the target ion increases; it is also suitable for dealing with a number of transitions in an economical fashion, a consideration that can not be ignored.

II. Method of Calculation

The method of distorted waves was used to obtain collision parameters for all transitions. In an LS coupling scheme, the excitation cross section between atomic terms $\alpha LS \rightarrow \alpha' L' S'$ is written as

$$Q(\alpha LS \rightarrow \alpha' L' S') = \frac{\Omega(\alpha LS, \alpha' L' S')}{E(2L+1)(2S+1)} \pi a_o^2 , \quad (1)$$

where E is the energy in Rydbergs of the incident electron and $\Omega(\alpha LS, \alpha' L' S')$ is the collision strength which is symmetric with respect to αLS and $\alpha' L' S'$.

A discussion of the method used in these calculations is presented in Ref. (1) and we refer the reader there for the details. As in Ref. (1), we made the following simplifying assumptions: Wave functions of the target ions were represented by LS coupling and we have omitted effects of configuration mixing, the electron exchange was taken into account only for collisions with helium-like Si XIII, in the expansion of the expression for the interaction potential, we have retained only terms corresponding to multipole orders lower than 3.

Although the collision strength is the fundamental atomic parameter, the result required for the interpretation of observed spectra is the collision strength averaged over an appropriate velocity distribution. For plasma electrons described by a Maxwellian velocity distribution function f(v) and electron temperature T, the excitation rate coefficient can be written as

$$X_{\alpha\beta}(T) = \int f(v)\, v\, Q_{\alpha\beta}(v)\ \text{cm}^3/\text{sec}. \quad (2)$$

In terms of the collision strength, the rate becomes

$$X_{\alpha\beta}(T) = \frac{8.63 \times 10^{-6}}{\omega_\alpha T^{\frac{1}{2}}} \int_{E_o/kT}^{\infty} \Omega \exp(-E/kT)\, d(E/kT), \qquad (3)$$

where ω_α and E_o is the statistical weight of level α and E_o is the excitation energy. Results will be presented for both the collision strength and excitation coefficient.

III. Results

The charge states, transitions, wavelengths and line strengths for which we have performed calculations are presented in Table 1. The target-ion ground-state wave functions are of the Hartree-Fock type, as given by Clementi.[2] The excited-state wave functions are obtained from a semi-empirical method using experimental eigenvalues when available; otherwise, theoretical estimates are used. The method generates radial wave functions, which are obtained in the field of a screened atomic potential and a statistical exchange potential with a variable parameter that guarantees the proper asymptotic behavior. In order to ensure that the radial functions satisfy the orthogonality condition, the method of undetermined Lagrange multipliers is utilized in a self-consistent fashion with the radial function routine.

After generating the excited-state wave functions, we formed the dipole matrix elements (or dipole-transition integral) and obtained estimates for the line strength. These results are presented in Table 1 along with some values quoted by Wiese et al[3] given in parentheses. For those transitions where a comparison could be made, the agreement is

reasonably good. Differences are probably caused by the effect of configuration mixing, which was ignored in our calculation. In addition, we have also listed the quadrupole-transition integral where appropriate. For convenience, we give the relationship between the spontaneous decay rate A and the line strength S (atomic units) for dipole transitions only [see Ref. (3) for quadrupole transitions, etc.], viz.

$$A = \frac{2.026 \times 10^{18}}{\tilde{\omega} \lambda^3} \quad S \quad (\text{sec}^{-1}) , \tag{4}$$

where $\tilde{\omega}$ is the statistical weight of the upper level and λ is the wavelength in angstrom units.

The results of the collision strength calculations are presented in Figs. 1 through 7 as functions of incident electron energy normalized with respect to the excitation energy, E_o, of the transition. The curves in the various figures are numbered in accordance with their entry in Table 1. For example, curve 1 in Fig. 1 refers to the $2p^5\ ^2P\text{-}2p^4(^3P)3d\ ^2D$ transition of Si, VI and is identified as such by referring to the column labeled "CODE" in Table 1. A review of the figures indicates that the collision strength is fairly constant for the $\Delta n = 0$ transitions but varies considerably otherwise, particularly for the spin exchange excitations.

Some caution must be exercised in interpreting the results presented in Table 1. The designation of a J value in the description of a transition is used only to identify the value of the energy level used in the calculation. We have not calculated collision parameters for J-J'

transitions. The results in the Table refer to the multiplet average. However, the results can be transformed easily to yield such information, provided that we neglect small energy differences of J sublevels.

For dipole transitions,

$$\Omega(SLJ,SL'J') = \begin{Bmatrix} 1 & J & J' \\ S & L' & L \end{Bmatrix}^2 \Omega(SL,SL') \frac{(2J+1)(2J'+1)}{2S+1}, \qquad (5)$$

and, if $S = 0$ or $L = 0$, then generally

$$\Omega(SLJ,S'L'J') = \frac{2J'+1}{(2S+1)(2L+1)} \Omega(SL,S'L').$$

The excitation rates were obtained from eqn. (5). For regions exceeding the range of our calculation, Ω was assumed to be constant. This procedure introduces only a small error into the excitation rate.

The majority of rate calculations can be represented adequately by a parametric fit of the form

$$X = \alpha e^{-\beta/T} T^{-\gamma}, \qquad (6)$$

where α, β and γ are the fitted parameters and the electron temperature T is in ev. We have divided the results into two groups. In the first group, we have set $\gamma = \frac{1}{2}$ with the values for α and β shown in Table 1. The fit was considered good when it reproduced the calculated values to within 20% over a temperature range of 100 to 10 kev. The second group of rates are predominantly intersystem transitions. Since a single value of γ would not represent the rate over the temperature range of interest, the results are presented graphically in Figs. 8 and 9.

IV. Summary

We have calculated line strengths, collision strengths and rate coefficients for a variety of transitions in multicharged silicon ions from Si VI to Si XIV. The line strengths were obtained by using Clementi wave functions for the ground-state configurations and excited-state wave functions generated by a semi-empirical method. For those cases where comparisons could be made, the agreement was good. The collision strengths were calculated in an LS coupling scheme in the distorted-wave approximation, neglecting exchange except for the helium-like transitions. These results were then integrated over a Maxwellian velocity distribution function to yield rate coefficients. The rates were presented either graphically or in terms of a two-parameter fit. Because of the paucity of both experimental and theoretical data for multicharged ions, we have been unable to make comparisons with other studies to judge the accuracy of our calculations. These results will be compared in a forthcoming paper with those currently under investigation using multiconfigurational wave functions.

Acknowledgements

This work was supported in part by the E. O. Hulbert Center for Space Research, NRL, as part of the ATM Data Analysis funded by NASA and by the Laboratory for Laser Energetics, University of Rochester.

References

1. J. Davis, P. C. Kepple, and M. Blaha, JQSRT 16, 1043 (1977).
2. E. Clementi, IBM Journal of Res. and Dev. 9, 2 (1965).
3. W. Wiese, M. Smith, and B. Miles, "Atomic Transition Probabilities," NBS 22, Vol. 1 (1966).

Appendix

In a previous paper[1] the following misprints should be corrected:

Table 3, the last line: the values 8.9 and 1230.0 should be replaced by 8.9(-10 and 12300.0, respectively.

Equation (21), the last line: ℓ_2 in the second 3-j symbol should be replaced by ℓ_2^1.

The titles of Figs. 7 and 8 should be interchanged.

Equation (18) symbol L_λ^d should be replaced by I_λ^d.

Charge	Transition	λ(Å)	α	β	S	Code
VI	$2p^5\ ^2P$ - $2p^4(^3P)3d\ ^2D$	83.3	8.41^{-9}	2.34^2	3.15^{-1}	1
	- $2p^4(^1S)3s\ ^2S$	91.4	2.06^{-10}	2.59^2	1.10^{-2}	2
	- $2p^4(^1D)3s\ ^2D$	96.0	1.48^{-9}	2.42^2	7.32^{-2}	3
	- $2p^4(^3P)3s\ ^2P$	99.5	1.62^{-9}	1.74^2	4.08^{-2}	4
VII	$2p^4\ ^3P$ - $2p^3(^4S)3d\ ^3D$	73.1	2.10^{-8}	2.62^2	1.10	5
	- $(^2D)3s\ ^3D$	81.6	1.23^{-9}	2.87^2	9.47^{-1}	6
VIII	$2p^2\ ^4S$ - $2p^3(^3P)3d\ ^4P$	61.1	4.96^{-8}	3.21^2	1.15	7
	- $(^3P)3s\ ^4P$	69.9	2.18^{-9}	3.33^2	7.25^{-1}	8
IX	$2p^2\ ^3P$ - $2p3d\ ^3D$	55.36	Figure 8		1.34	9
	- $2p3p\ ^3D$	55.36	5.15^{-8}	4.05^1	1.14	10
	- $2s2p^3\ ^3S$	225.03	3.85^{-8}	6.36^1	$9.46^{-1}(6.7^{-1})$	11
	- $2s2p^3\ ^3P$	292.83	3.01^{-8}	4.81^1	$6.92^{-1}(7.9^{-1})$	12
	- $2s2p^3\ ^3D$	345.1	5.15^{-8}	4.05^1	$1.14\ (1.86^{-1})$	13
X	$2p\ ^2P_{3/2}$ - $6d\ ^2D_{5/2}$	34.24	8.51^{-10}	4.70^2	1.72^{-2}	14
	- $5d\ ^2D_{5/2}$	35.39	1.54^{-9}	4.67^2	3.58^{-2}	15
	$2p\ ^2P_{1/2}$ - $4d\ ^2D_{3/2}$	39.44	3.80^{-9}	4.41^2	9.96^{-2}	16
	- $4s\ ^2S_{1/2}$	40.41	1.00^{-10}	5.20^2	3.76^{-3}	17
	- $3d\ ^2D_{1/2}$	50.52	1.81^{-8}	3.74^2	$5.98^{-1}(6.3^{-1})$	18
	$2p\ ^2P_{3/2}$ - $3s\ ^2S_{1/2}$	55.10	4.70^{-10}	4.01^2	2.27^{-2}	19
	$2s^2 2p\ ^2P_{1/2}$ - $2s2p^2\ ^2D_{3/2}$	347.43	4.86^{-8}	4.00^1	$7.13^{-1}(5.1^{-1})$	20
XI	$2s^2\ ^1S_o$ - $2s5d\ ^1D_2$	30.23	8.94^{-10}	4.56^2	3.74^{-2} *	21
	-$2s5p\ ^1P_1$	30.37	Figure 8		6.45^{-3}	22
	-$4d\ ^1D_2$	33.25	2.40^{-9}	4.28^2	8.01^{-2}*	23

Charge	Transition	λ(Å)	α	β	S	Code
XI	$2s^2\ ^1S_0$ - $2s4p\ ^1P_1$	33.52	Figure 8		1.72^{-2}	24
	- $2s3d\ ^1D_1$	42.35	1.30^{-8}	4.02^{2}	3.56^{-1}*	25
	- $2s3p\ ^1P_1$	43.76	Figure 8		8.73^{-2}	26
	- $2s2p\ ^1P_1$	303.31	1.57^{-7}	4.60^{1}	$3.87^{-1}(2.64^{-1})$	27
XII	$2s\ ^2S_{1/2}$ - $5p\ ^2P_{3/2}$	27.42	5.04^{-10}	7.55^{2}	6.49^{-3}	28
	- $4p\ ^2P_{3/2}$	31.02	1.34^{-9}	6.73^{2}	1.78^{-2}	29
	- $2d\ ^2D$	40.59	6.84^{-9}	3.75^{2}	3.23^{-1}*	30
	- $3p\ ^2P_{3/2}$	40.91	5.49^{-9}	5.38^{2}	9.28^{-2}	31
	- $3s\ ^2S$	41.83	2.55^{-9}	2.87^{2}		32
	- $2p\ ^2P_{3/2}$	499.37	7.91^{-8}	2.72^{1}	$3.58^{-1}(3.60^{-1})$	33
XIII	$1s^2\ ^1S$ - $1s4p\ ^1P$	5.41	Figure 9		1.06^{-3}	34
	- $1s3p\ ^1P$	5.68	Figure 9		2.85^{-3}	35
	- $1s2p\ ^1P$	6.65	Figure 9		1.69^{-2}	36
	- $1s2p\ ^3P$	6.69	Figure 8			37
	- $1s2s\ ^3S$	6.74	Figure 8			38
	$1s2s\ ^3S$ - $1s2p\ ^1P$	515.0	Figure 9			39
XIV	$1s\ ^2S$ - $2p\ ^2P$	6.18	Figure 9		$1.70^{-2}(1.70^{-2})$	40

. $8.41^{-9} = 8.41 \times 10^{-9}$

* quadrupole transition integral

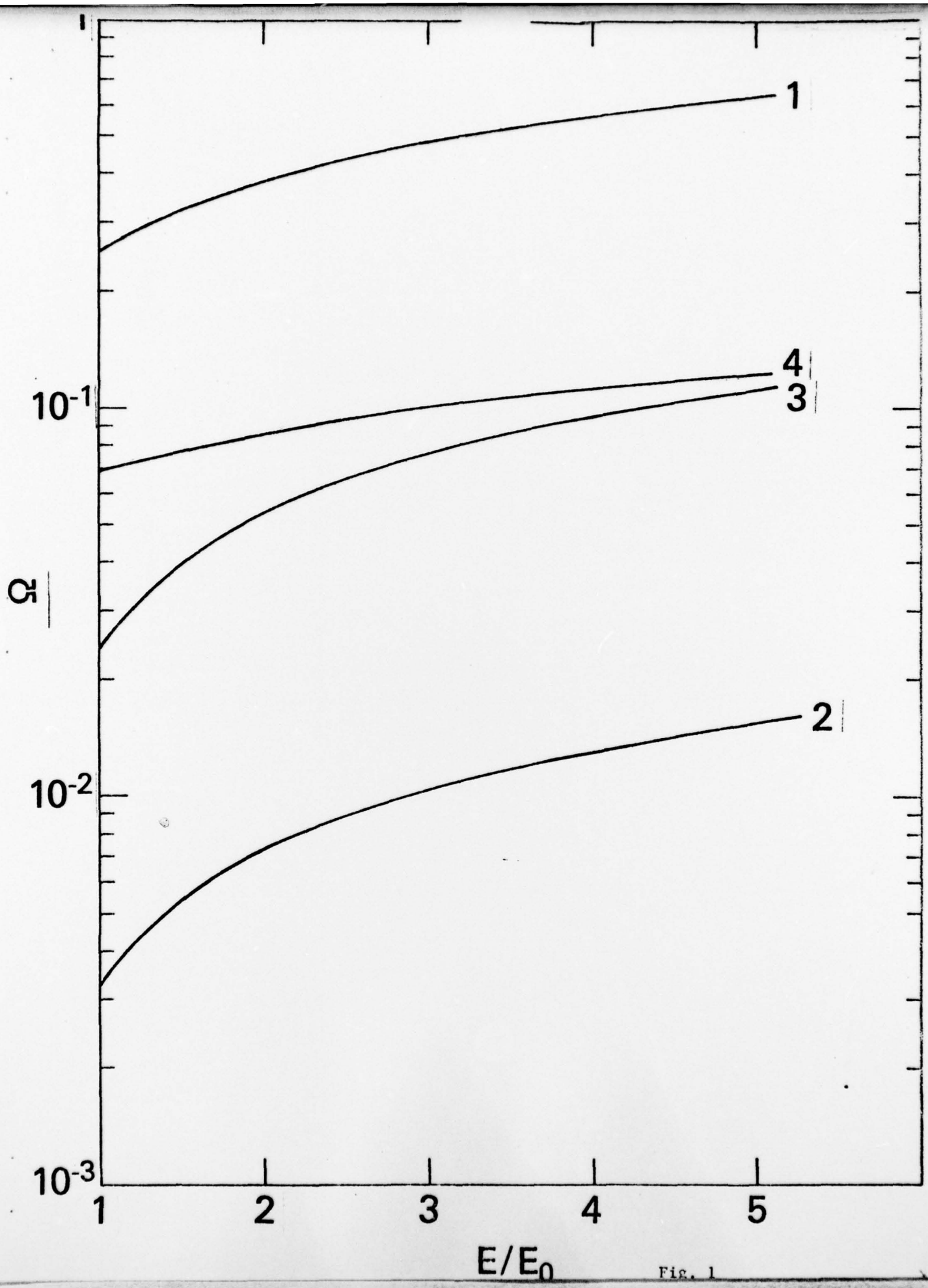

Fig. 1

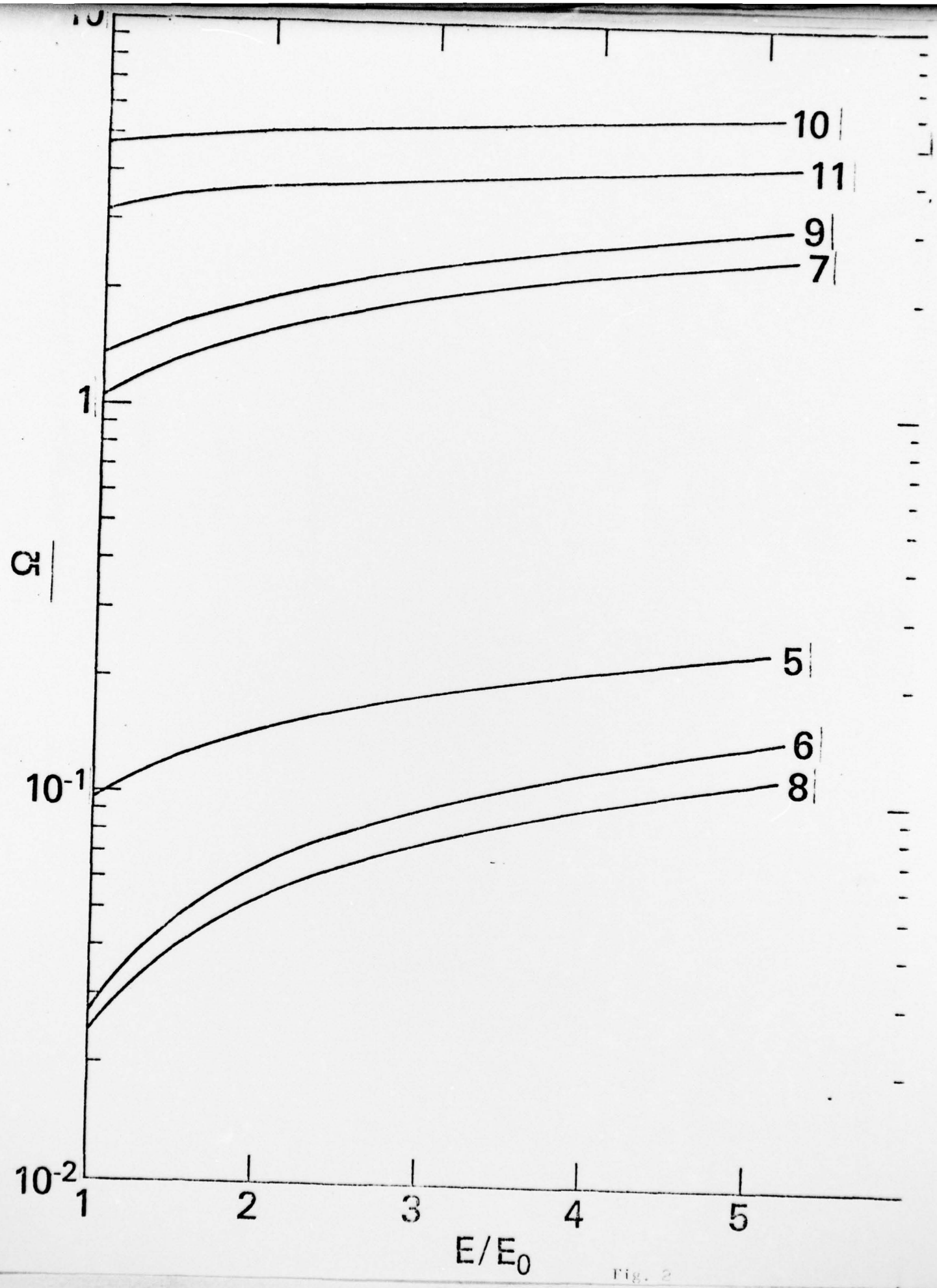

Fig. 2

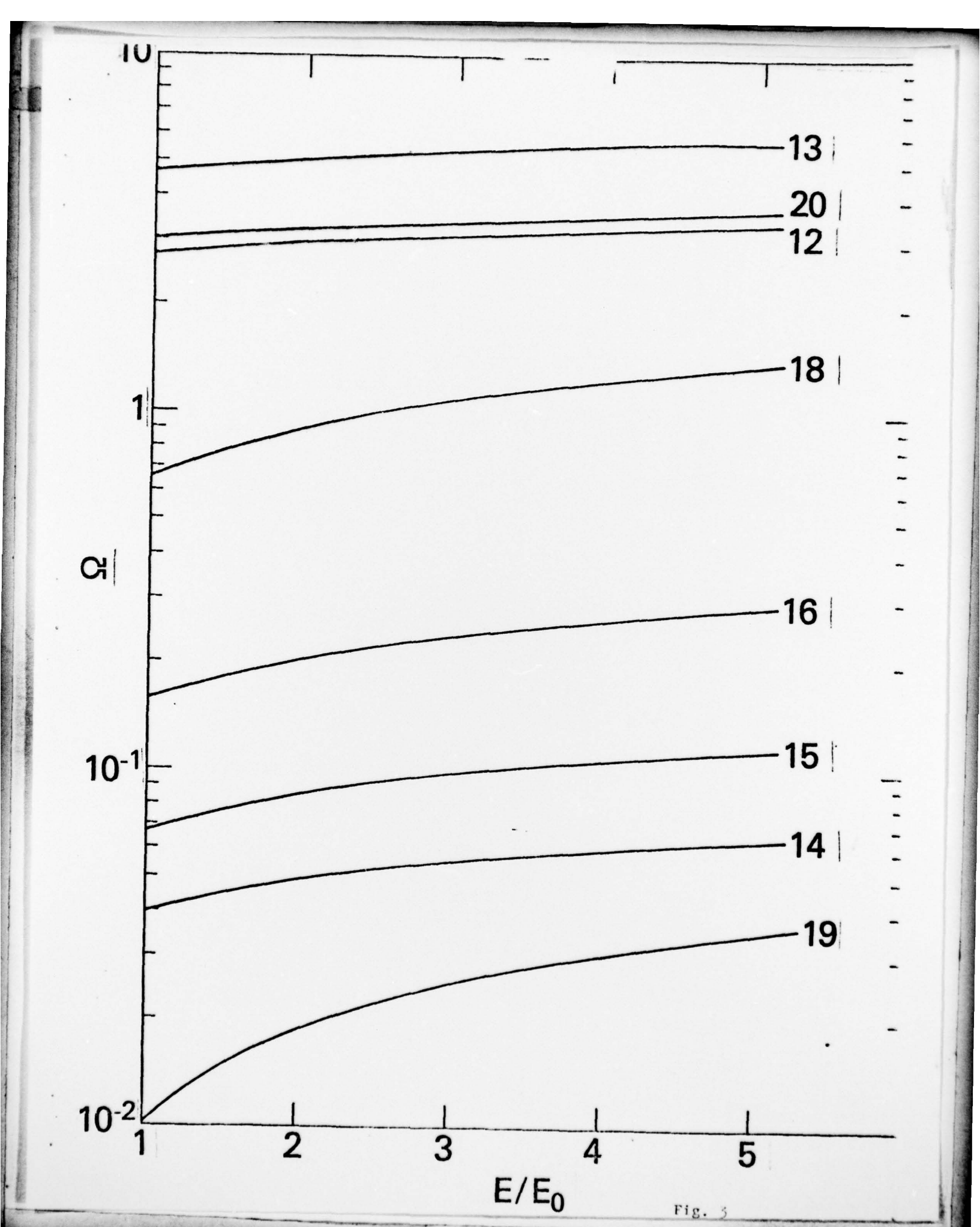

Fig. 3

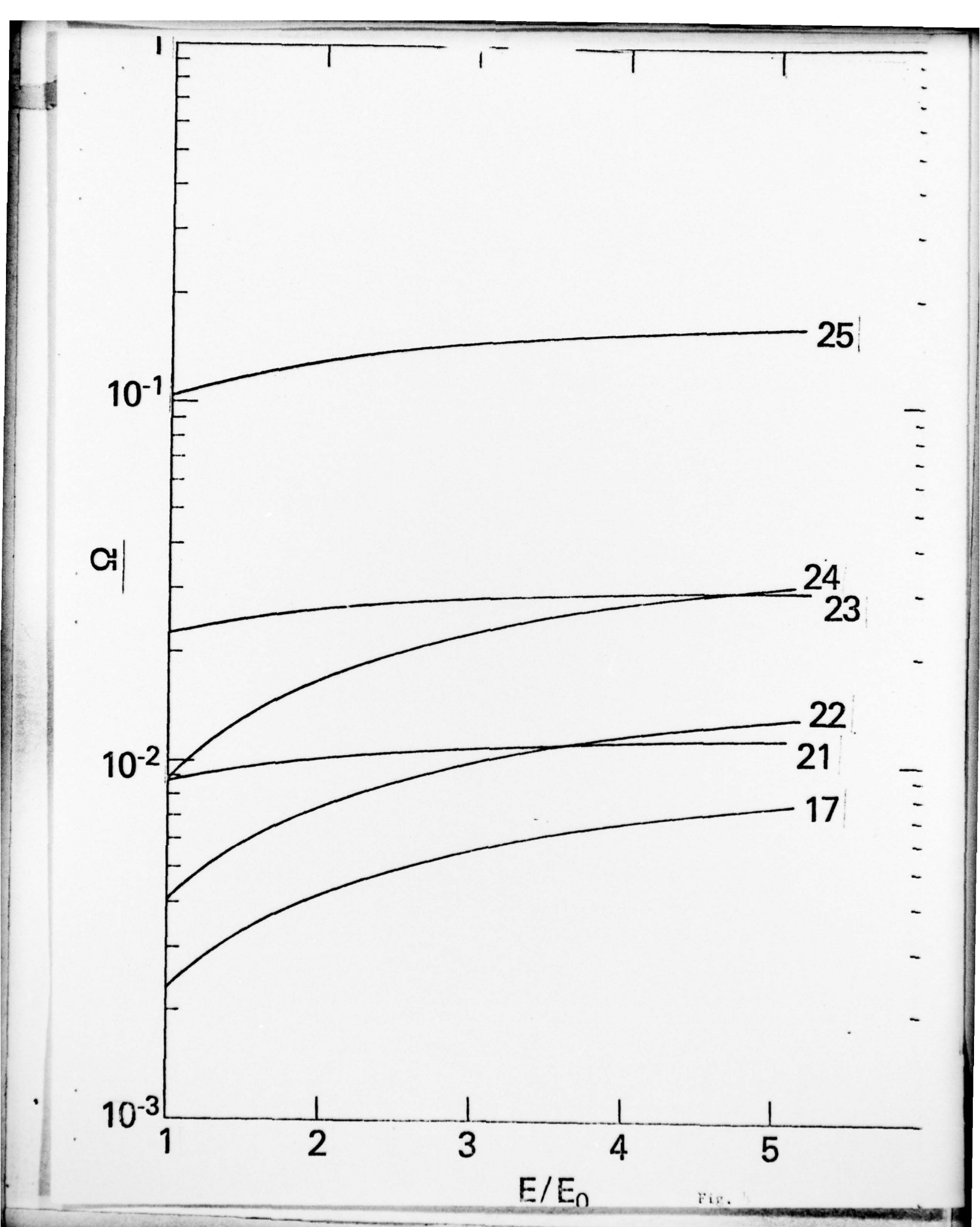

Fig.

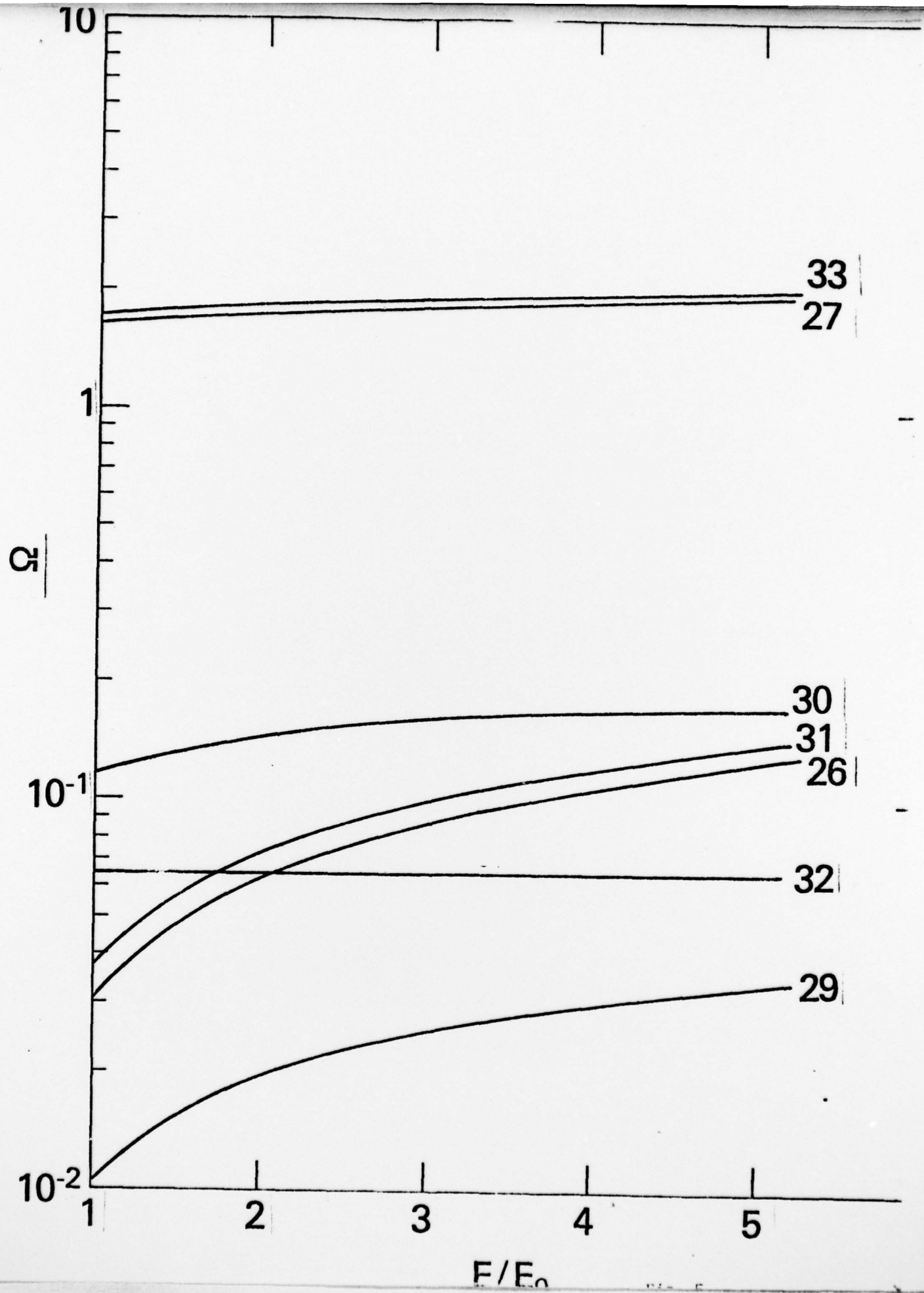
10
1
10^{-1}
10^{-2}
α
33
27
30
31
26
32
29
1
2
3
4
5
E/E_0

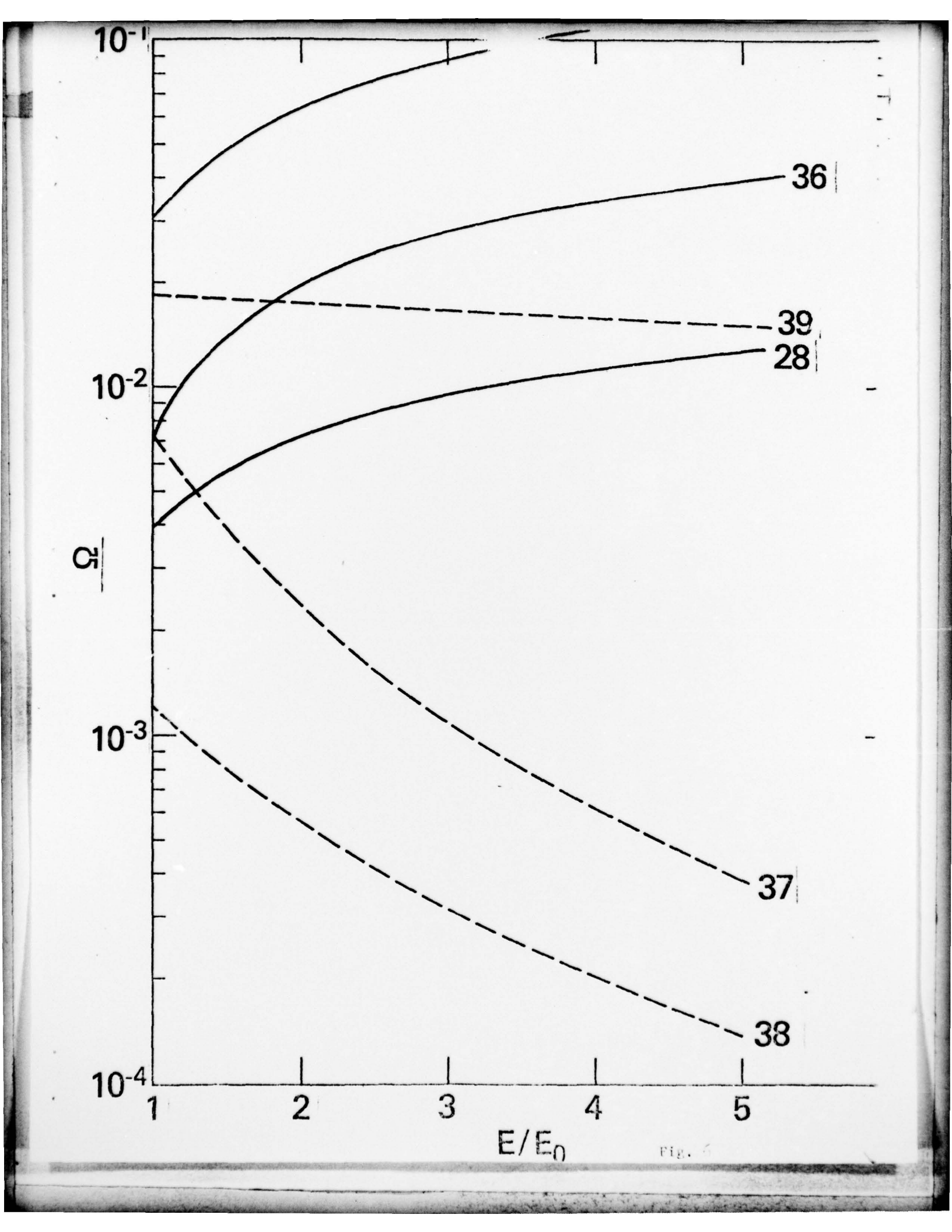

Fig. 4

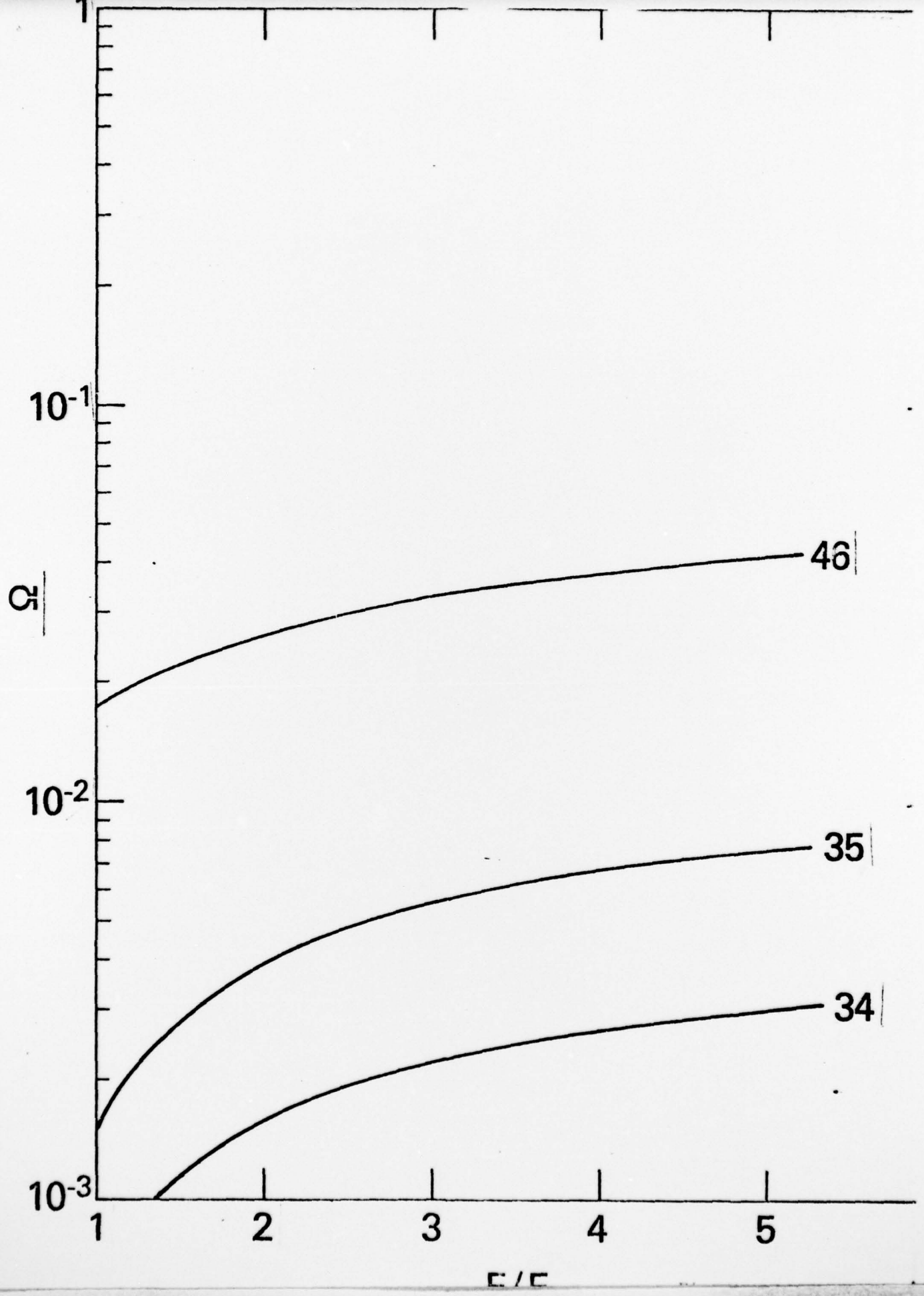
1
10^{-1}
10^{-2}
10^{-3}
Cl
46
35
34
1
2
3
4
5
E/E

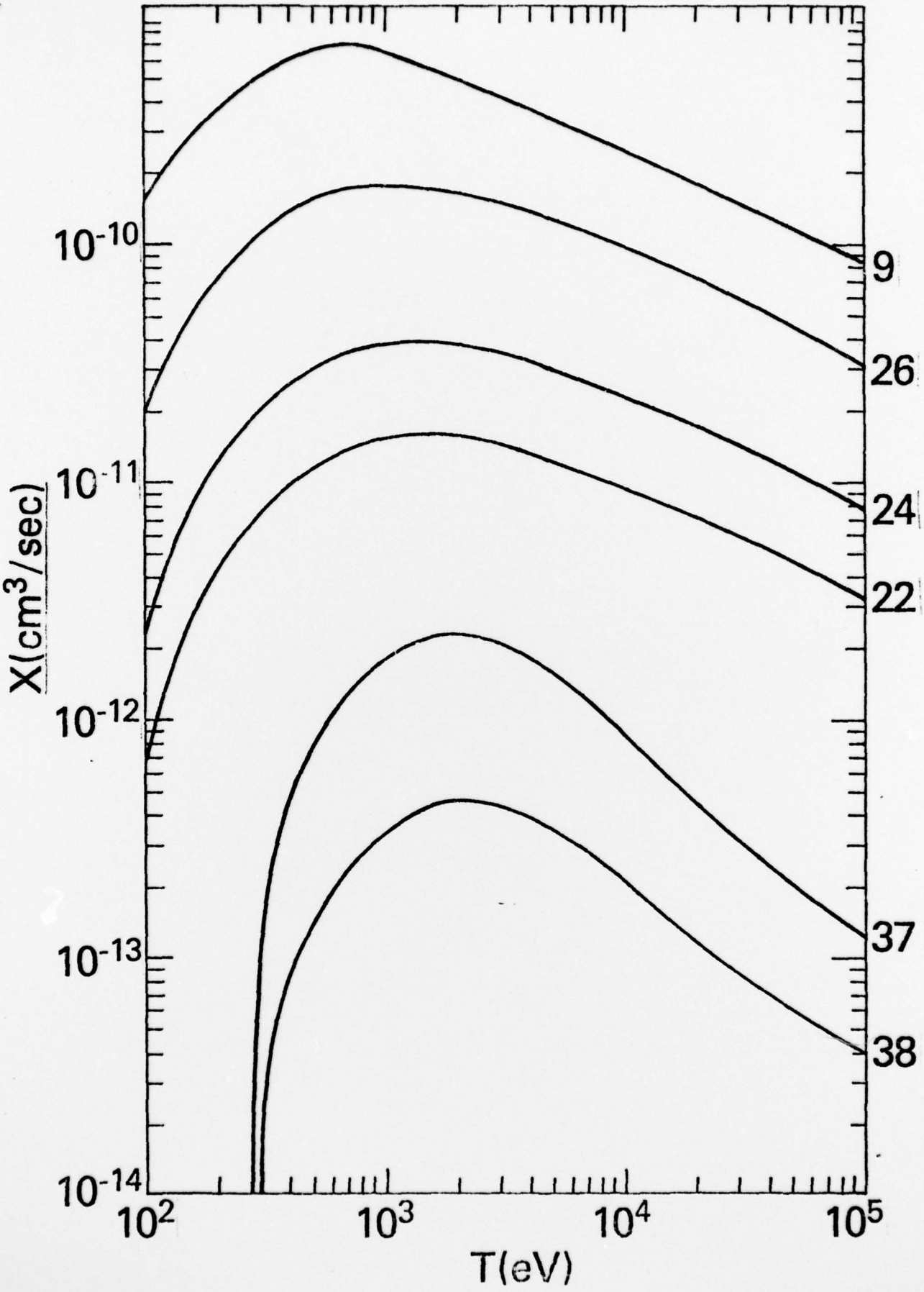
10^{-10}
10^{-11}
10^{-12}
10^{-13}
10^{-14}
X(cm³/sec)
9
26
24
22
37
38
10^2
10^3
10^4
10^5
T(eV)

Fig. 8

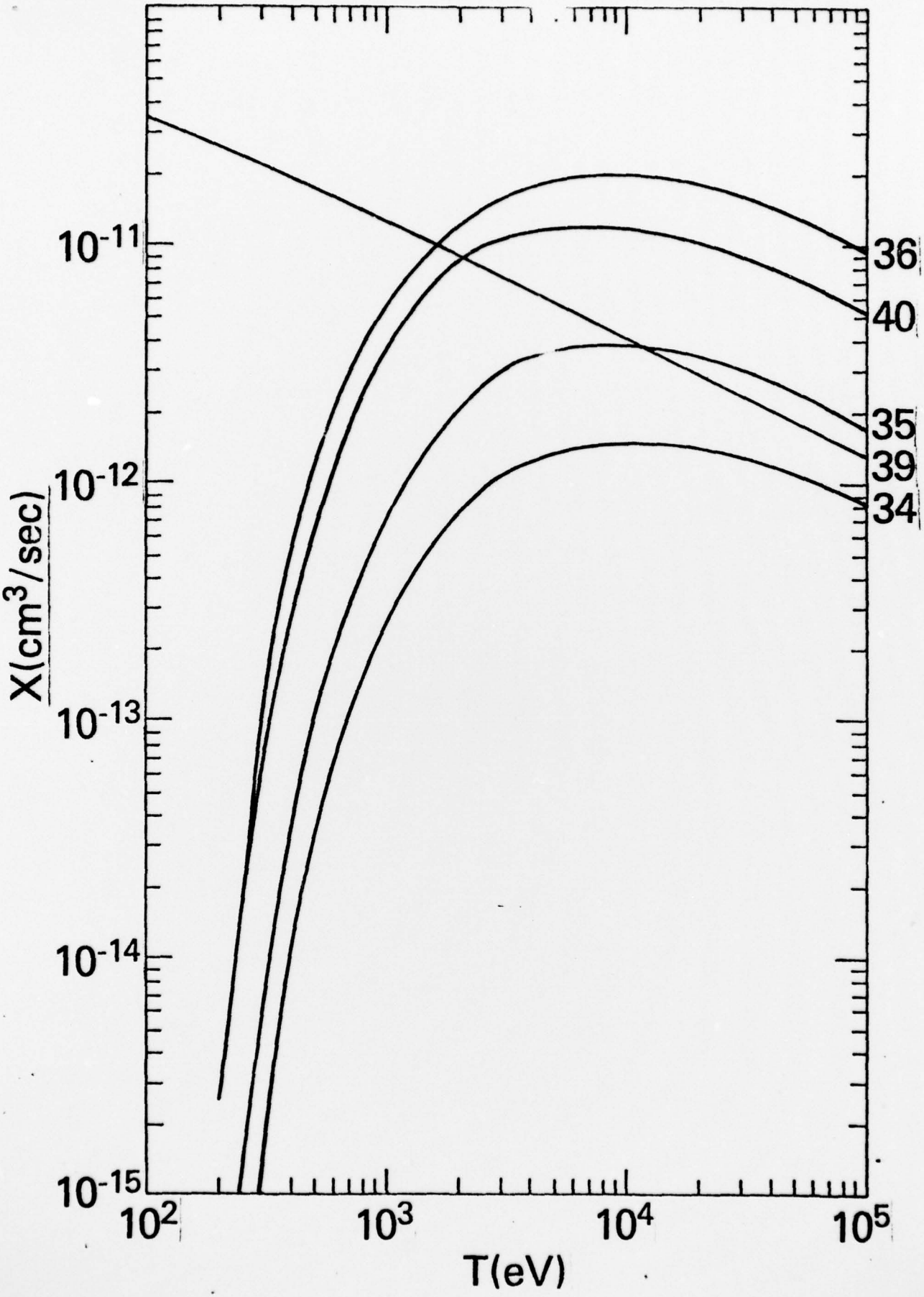
10^{-11}
10^{-12}
10^{-13}
10^{-14}
10^{-15}
X(cm³/sec)
10^2
10^3
10^4
10^5
T(eV)
36
40
35
39
34

Fig. 9